Centrum voor Wiskunde en Informatica
REPORT*RAPPORT*

Sensitivity of Atmospheric Transport Model Performance to Numerical Advection Schemes and Resolution

E.J. Spee, A.C. Petersen, H. van Dop, W.H. Hundsdorfer

Modelling, Analysis and Simulation (MAS)

MAS-R9710 March 31, 1997

Report MAS-R9710
ISSN 1386-3703

CWI
P.O. Box 94079
1090 GB Amsterdam
The Netherlands

Sensitivity of Atmospheric Transport Model Performance to Numerical Advection Schemes and Resolution

E. J. Spee
Centre for Mathematics and Computer Science (CWI)
P.O. Box 94079, 1090 GB Amsterdam, The Netherlands
Edwin.Spee@cwi.nl

A. C. Petersen
Institute for Marine and Atmospheric Research Utrecht (IMAU)
Utrecht University, P.O. Box 80005, 3508 TA Utrecht, The Netherlands
A.C.Petersen@fys.ruu.nl

H. van Dop
IMAU
H.vanDop@fys.ruu.nl

W. Hundsdorfer
CWI
W.Hundsdorfer@cwi.nl

ABSTRACT

We have tested four newly developed 3D advection schemes named Mol-rg, Split-u, Split-us and Split-rg. We compared these schemes with Slopes and Second Moment. Mol-rg and Split-rg make use of a reduced grid, a grid with less cells near the poles, to overcome the well known pole-singularity.

Two tests were performed with all schemes: the solid-body rotation test and a radon test. The radon test uses 3D meteorological input for the month January 1992 from a numerical weather prediction model, together with parametrizations for sub-grid scale vertical transport. We compared model results with measurements on three islands in the Indian Ocean.

From the solid-body rotation test we learn that all new schemes do not generate undershoot and overshoot and are mass conservative. Split-us and Split-rg are very cheap in terms of CPU time and memory requirements and give accurate results.

The model results for the radon test give good predictions for the background concentration. However, the correlation between measured and simulated radon concentration peaks is poor for the simulated period. The model results are found to be almost independent of the numerical scheme used, but depend mostly on the resolution and the quality of meteorological input. Therefore it is important to use cheap advection schemes such as Split-rg to be able to perform model calculations on high resolutions.

The new advection schemes are available through Internet.

1991 Mathematics Subject Classification: 65M06, 65M20, 65Y20 and 86A10
1991 Computing Reviews Classification System: G.1.7 and G.1.8
Keywords and Phrases: Hyperbolic PDEs; Linear advection; Global atmospheric models
Note: Work was carried out under project CIRK in MAS1 and was supported by GOA and RIVM.

1. Introduction

Due to non-linearity of chemistry and spatial heterogeneity of anthropogenic trace gas sources, a trend towards the use of higher resolutions in global tropospheric chemistry modeling can be recognized. For models designed to run for several years with a large number of chemical species and using monthly averaged climatological meteorology, the horizontal resolution has recently increased from (longitude $\times$ latitude) $10^\circ \times 10^\circ$ in MOGUNTIA [*Crutzen and Zimmermann*, 1991] to $5^\circ \times 5^\circ$ in IMAGES [*Müller and Brasseur*, 1995]. At this moment both on-line models, which calculate the meteorology at every time step, and off-line models, which use climate or weather forecast model output at 4 to 12-hourly time resolution, typically use $5^\circ \times 5^\circ$ resolution to simulate tropospheric ozone and sulfur species [*Roelofs and Lelieveld*, 1995; *Feichter et al.*, 1996; *Chin et al.*, 1996]. *Roelofs and Lelieveld* [1995] plan to use T42 resolution (approximately $3^\circ \times 3^\circ$) in the future in order to simulate middle and high latitude stratosphere-troposphere exchange more realistically. According to *Peters et al.* [1995] grid resolutions of $0.5^\circ \times 0.5^\circ$ or better in the horizontal are needed for an adequate modeling of anthropogenic perturbations to global atmospheric chemistry.

This paper addresses the computational aspects involved in increasing the resolution of present-day on-line and off-line atmospheric chemistry models. We focus on the cost of numerical solution of the advection equation which for most schemes increases more rapidly for higher resolutions than the numerical solution of the chemistry equations. This is due to the CFL constraint on the advection time step. We investigate several aspects of the performance of two widely used advection schemes (Slopes [*Russell and Lerner*, 1981] and Second Moment [*Prather*, 1986]) and four new schemes (named Split-rg, Split-u, Split-us and Mol-rg) at horizontal resolutions varying from $5.6^\circ \times 5.6^\circ$ to $1.4^\circ \times 1.4^\circ$. The sensitivity of the performance to variations in resolution is examined and implications for performance at higher resolutions than $1.4^\circ \times 1.4^\circ$ are formulated. The performance of the schemes is both tested with idealized numerical tests and with a radon test for horizontal transport. For the latter test we have implemented the four new schemes in the KNMI version of the TM2 model, described in [*Heimann*, 1995; *Velders et al.*, 1994]. We used one month of 12-hourly assimilated meteorological observations (ECMWF's initialized analyses) at resolutions of $5.0^\circ \times 3.8^\circ$ and $2.5^\circ \times 2.5^\circ$ to drive the off-line model in order to compare the model results for different numerical schemes with measurements at three Indian Ocean sites.

2. Model description and operator splitting

The basic equation in atmospheric transport modeling is the balance equation

$$\frac{\partial c}{\partial t} + \nabla(\vec{u}c) = R(c) + S(c). \tag{2.1}$$

The unknown c denotes a vector of species concentration, say of length n. The velocity wind field vector $\vec{u}$ is given. The term S represent the parametrized sub-grid scale transport in the vertical direction. The term R represents source and sink terms. In hybrid coordinates, with some commonly used assumptions, Equation (2.1) transforms into

$$\frac{\partial c}{\partial t} + \frac{1}{a\cos\phi}\left[\frac{\partial(u\,c)}{\partial\lambda} + \frac{\partial(v\,c\,\cos\phi)}{\partial\phi}\right] + \frac{1}{h_\eta}\frac{\partial(w\,c)}{\partial\eta} = R(c) + S(c), \tag{2.2}$$

with λ, ϕ and η the coordinates in the longitudinal, latitudinal and vertical direction, u, v and w are the velocity components in the λ, ϕ and η direction, and h_η is a scale factor from the coordinate transformation.

2.1 Operator splitting

We rewrite Equation (2.2) into

$$\frac{\partial c}{\partial t} = A(c) + R(c) + S(c), \tag{2.3}$$

where $A(c)$ is the advection operator in hybrid coordinates. This equation is normally solved using operator splitting, mainly to treat advection explicit, and (stiff) chemistry implicit. It also gives the possibility to use different time steps for different operators and different areas. We use the symmetric *Strang* [1968] operator splitting,

$$\frac{\partial}{\partial t}c^{(1)}(t) = A(c^{(1)}(t)) \qquad (t_s \le t \le t_{s+\frac{1}{2}}), \qquad c^{(1)}(t_s) = c_s, \tag{2.4a}$$

$$\frac{\partial}{\partial t}c^{(2)}(t) = R(c^{(2)}(t)) \qquad (t_s \le t \le t_{s+\frac{1}{2}}), \qquad c^{(2)}(t_s) = c^{(1)}(t_{s+\frac{1}{2}}), \tag{2.4b}$$

$$\frac{\partial}{\partial t}c^{(3)}(t) = S(c^{(3)}(t)) \qquad (t_s \le t \le t_{s+1}), \qquad c^{(3)}(t_s) = c^{(2)}(t_{s+\frac{1}{2}}), \tag{2.4c}$$

$$\frac{\partial}{\partial t}c^{(4)}(t) = R(c^{(4)}(t)) \qquad (t_{s+\frac{1}{2}} \le t \le t_{s+1}), \quad c^{(4)}(t_{s+\frac{1}{2}}) = c^{(3)}(t_{s+1}), \tag{2.4d}$$

$$\frac{\partial}{\partial t}c^{(5)}(t) = A(c^{(5)}(t)) \qquad (t_{s+\frac{1}{2}} \le t \le t_{s+1}), \quad c^{(5)}(t_{s+\frac{1}{2}}) = c^{(4)}(t_{s+1}), \tag{2.4e}$$

where c_s is an approximation to the exact concentration vector c at $t = t_s$ and $c_{s+1} \equiv c^{(5)}(t_{s+1})$ at $t = t_{s+1}$. We use $\Delta t_{split} = t_{s+1} - t_s = 1\,hour$.

2.2 Solving the sub-grid scale parametrization

Equation (2.4c) solves ECMWF's parametrizations for sub-grid scale vertical transport, based on the cumulus clouds calculation by the mass flux scheme of *Tiedtke* [1989] and the vertical diffusion coefficients calculated by the stability of the air using the formulae of *Louis* [1979].

$$\frac{\partial\,(c)}{\partial t} = S\,(c) = -\frac{\partial}{\partial \eta}F_S, \tag{2.5}$$

where F_S is the sub-grid scale tracer flux. As in [*Heimann*, 1995] we integrate Equation (2.5) over a grid box at height level k and obtain

$$\frac{d}{dt}n_k = \left(F_{S,k-\frac{1}{2}} - F_{S,k+\frac{1}{2}}\right), \tag{2.6}$$

where the tracer mass n_k in the vertical column (i, j) is equal to $V_{(i,j,k)}\,c_{(i,j,k)}$, with V the volume of the grid cell. The flux $F_{S,k+\frac{1}{2}}$ depends on the tracer mass in all layers,

$$F_{S,k+\frac{1}{2}} = \sum_{l=1}^{\mathrm{NS}} f_{k+\frac{1}{2},l}\,n_l, \tag{2.7}$$

where $l = 1$ is the top level and $l = \mathrm{NS}$ is the ground level. The coefficients $f_{k+\frac{1}{2},l}$ represent the fraction of tracer mass of layer l that, per unit of time, crosses the layer boundary $k + \frac{1}{2}$ by means of sub-grid scale vertical transport processes. On the reduced grid these coefficients (available from meteorological input on the uniform grid) are averaged over the combined cells. So we have

$$\frac{d}{dt}\vec{n} = \mathbf{M}\cdot\vec{n}, \tag{2.8}$$

where the elements of the matrix $\mathbf{M}$ are given as

$$[\mathbf{M}]_{k,l} = f_{k-\frac{1}{2},l} - f_{k+\frac{1}{2},l}. \tag{2.9}$$

The dimension of the matrix $\mathbf{M}$ is NS=15, the number of vertical layers. Equation (2.8) is solved fully implicitly

$$\vec{n}(t+\Delta t_S) = \vec{n}(t) + \Delta t_S\mathbf{M}\cdot\vec{n}(t+\Delta t_S) = (I - \Delta t_S\mathbf{M})^{-1}\vec{n}(t) = \mathbf{C}\cdot\vec{n}, \tag{2.10}$$

where Δt_S is equal to Δt_{split}. The matrix inversion, which gives the convection matrix $\mathbf{C}$, is done once per meteorological time step. The first order moments are updated as is done in TM [*Heimann*, 1995], and the second order moments are treated analogously (see section 3 for a short introduction and references on first and second order moments). The assumption is that all moments involving horizontal components retain their information and are mixed as the means, and that the moments involving only vertical components gradually lose their information during convection [*Prather et al.*, 1987].

2.3 Solving the source and sink terms

On the imposed grid, we have to solve in each grid point the ODE (Ordinary Differential Equation) (2.4b), which takes the specific form

$$V\,\rho\,\frac{d\chi}{dt} \;=\; P \;-\; V\,\rho\,k_1\,\chi \tag{2.11}$$

with χ the mixing ratio ^{222}Rn, P the emission ($kg\,s^{-1}$), ρ the density and the rate constant $k_1 = 2.0974\times10^{-6}\,s^{-1}$, which corresponds to the half-life time of 3.8 days. This ODE can be solved exactly:

$$V\,\rho\,\chi(t\,+\,\Delta t_R) \;=\; V\,\rho\,e^{-k_1\,\Delta t_R}\,\chi(t) \;+\; \left(1-e^{-k_1\Delta t_R}\right)\frac{P}{k_1}, \tag{2.12}$$

with $\Delta t_R = \frac{1}{2}\,\Delta t_{split}$. The first and second order moments are updated as is done in the TM version in use at KNMI. They all have the same decay factor $e^{-k_1\,\Delta t_R}$, and the first order moment in the vertical direction at ground level is decreased due to emission at the bottom.

3. Numerical methods: advection schemes

The discretization of the advection equation on the grid (λ_i, ϕ_j, η_k) is determined by the wind field $\vec{u}$, which is in the radon test given as mass fluxes f, defined as:

$$f_{\lambda_{(i+\frac{1}{2},j,k)}} \;=\; \rho_{(i+\frac{1}{2},j,k)} * A_{\lambda_{(i+\frac{1}{2},j,k)}} * u_{(i+\frac{1}{2},j,k)}, \tag{3.13a}$$

$$f_{\phi_{(i,j+\frac{1}{2},k)}} \;=\; \rho_{(i,j+\frac{1}{2},k)} * A_{\phi_{(i,j+\frac{1}{2},k)}} * v_{(i,j+\frac{1}{2},k)}, \tag{3.13b}$$

$$f_{\eta_{(i,j,k+\frac{1}{2})}} \;=\; \rho_{(i,j,k+\frac{1}{2})} * A_{\eta_{(i,j,k+\frac{1}{2})}} * w_{(i,j,k+\frac{1}{2})}, \tag{3.13c}$$

with ρ the density of air, and A the area between two grid cells. If these mass fluxes are mass conserving, we have

$$\begin{aligned}\frac{d}{dt}m_{air_{(i,j,k)}} \;-\; \big((&f_{\lambda_{(i-\frac{1}{2},j,k)}} - f_{\lambda_{(i+\frac{1}{2},j,k)}}\big)\\ +\big(&f_{\phi_{(i,j-\frac{1}{2},k)}} - f_{\phi_{(i,j+\frac{1}{2},k)}}\big)\\ +\big(&f_{\eta_{(i,j,k-\frac{1}{2})}} - f_{\eta_{(i,j,k+\frac{1}{2})}}\big)\big) \;=\; 0.\end{aligned} \tag{3.14}$$

Using $m_{air} = V\,\rho$ and $\chi = c\,/\,\rho$ with V the volume and χ the mixing ratio, we obtain the advection equation with mass fluxes

$$\begin{aligned}V_{(i,j,k)}\,\frac{d}{dt}\left(\rho_{(i,j,k)}\chi_{(i,j,k)}\right) \;=\; \Big[&f_{\lambda_{(i-\frac{1}{2},j,k)}}\,\chi_{(i-\frac{1}{2},j,k)} - f_{\lambda_{(i+\frac{1}{2},j,k)}}\,\chi_{(i+\frac{1}{2},j,k)}\\ &+f_{\phi_{(i,j-\frac{1}{2},k)}}\,\chi_{(i,j-\frac{1}{2},k)} - f_{\phi_{(i,j+\frac{1}{2},k)}}\,\chi_{(i,j+\frac{1}{2},k)}\\ &+f_{\eta_{(i,j,k-\frac{1}{2})}}\,\chi_{(i,j,k-\frac{1}{2})} - f_{\eta_{(i,j,k+\frac{1}{2})}}\,\chi_{(i,j,k+\frac{1}{2})}\Big].\end{aligned} \tag{3.15}$$

We are comparing six numerical schemes for advection: two schemes presently used in the TM model, namely Slopes developed by *Russell and Lerner* [1981] and Second Moment developed by *Prather* [1986], and four new schemes. For ease of comparison we also include the Donorcell algorithm

on a reduced grid. Donorcell is first order in time and space, computational cheap, mass conservative, monotonic and therefore extremely diffusive.

The main difference between the advection schemes is the interpolation of χ to obtain the value at cell interfaces from cell center values. Donorcell and the new schemes use only cell center values, whereas Slopes uses also the first order moment (slope) of the mixing ratio, and Second Moment uses the first and second order moments of the mixing ratio (which explains there names). This results in different memory requirements for the last two schemes, see section 4.

The new schemes are all of explicit finite-volume type, with flux limiting to avoid negative values, or even better, avoid over- and undershoot. The flux limiters are based on formulas introduced by *van Leer* [1977], see also *Koren* [1993]. The 2D versions of the schemes are tested in [*Hundsdorfer and Spee*, 1995; *Blom et al.*, 1994; *Spee*, 1995]. The extension to 3D is given in Appendix A. In Appendix A we also introduce mixing ratio fluxes.

Other characteristics of the schemes:

Mol-rg A Method of Lines (MOL) scheme on a reduced grid. In the MOL approach the advection equation is first discretized in space, resulting in an ODE. For the time integration standard ODE solvers are used. Mol-rg uses ($\kappa = \frac{1}{3}$) discretization on a reduced grid, and a second order Runge-Kutta scheme viz. the explicit trapezoidal rule, for time integration [*Hundsdorfer et al.*, 1995].

Split-u a dimensional splitting scheme on a uniform grid, based on formulas derived in [*Hundsdorfer and Spee*, 1995]. The 1D subprocesses that arise within the splitting are solved using direct discretization [*Hundsdorfer and Trompert*, 1993]. Due to the term $\cos\phi$ in Equation 2.2, the CFL condition requires very small time steps on fine grids which makes this scheme very expensive in terms of CPU time. Therefore two modifications of Split-u are developed.

Split-us a modification of Split-u, where the longitudinal direction is made unconditionally stable by allowing the stencil to vary with the courant number. This is as with semi-Lagrangian methods, but due to the conservation form of the scheme we maintain the mass-conservation property [*Hundsdorfer and Spee*, 1995].

Split-rg a modification of Split-u, where the uniform grid is replaced by a reduced grid, as in Mol-rg.

The schemes are available through WWW.

The reduced grid [*Prather et al.*, 1987; *Williamson*, 1992; *Rasch*, 1994] is a uniform grid with less cells near the poles to overcome the polar singularity, see Figure 1 for an example. Grid reduction means that at a small number of latitudes near the poles the grid size in the longitudinal direction is doubled.

In the dimensional splitting schemes one advection step is a sequence of 1D advection steps:

method	Slopes, Second Moment and Split-u	Split-rg and Split-us
sequence	λ direction during $\frac{1}{4}\Delta t_{adv}$	
	ϕ direction during $\frac{1}{2}\Delta t_{adv}$	ϕ direction during $\frac{1}{2}\Delta t_{adv}$
	λ direction during $\frac{1}{4}\Delta t_{adv}$	λ direction during $\frac{1}{2}\Delta t_{adv}$
	η direction during Δt_{adv}	η direction during Δt_{adv}
	λ direction during $\frac{1}{4}\Delta t_{adv}$	λ direction during $\frac{1}{2}\Delta t_{adv}$
	ϕ direction during $\frac{1}{2}\Delta t_{adv}$	ϕ direction during $\frac{1}{2}\Delta t_{adv}$
	λ direction during $\frac{1}{4}\Delta t_{adv}$	

The sequence is chosen such that we have a symmetric *Strang* [1968] splitting and for each direction

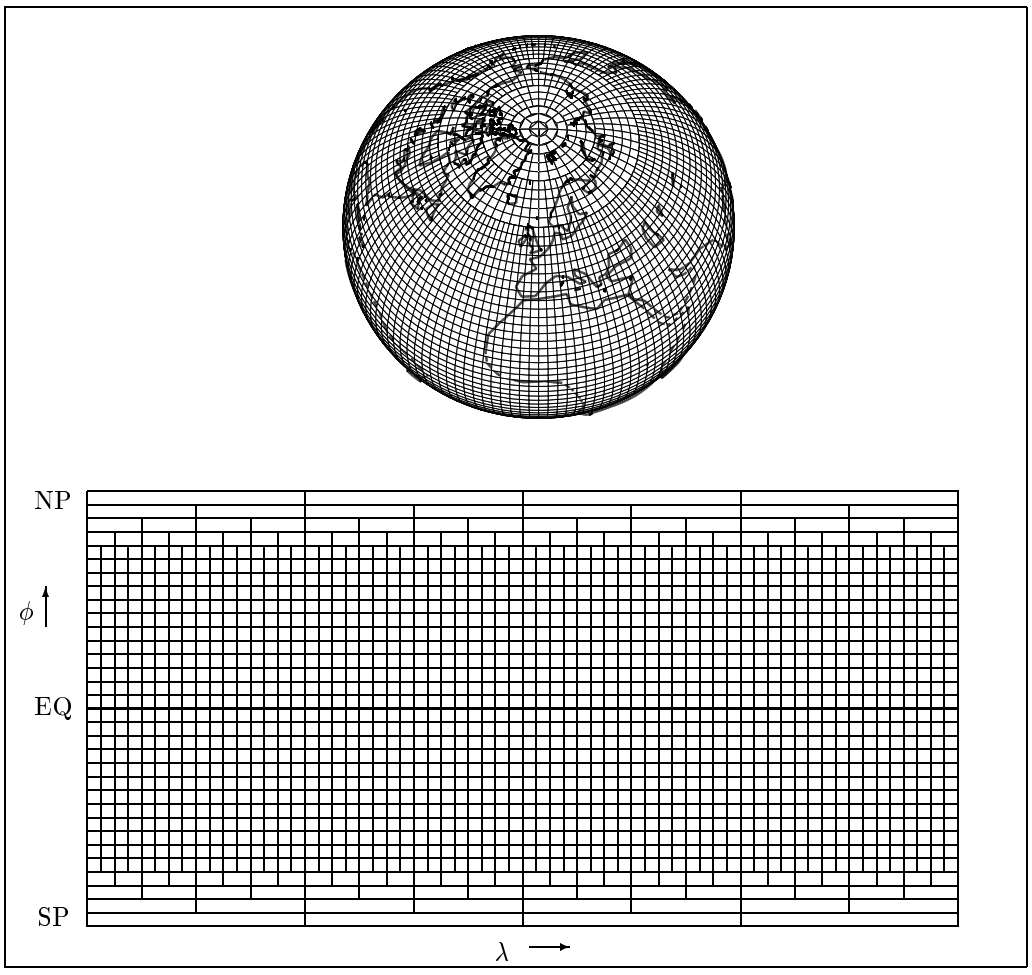

Figure 1: A reduced grid on the globe (top), and a 64×32 reduced grid in longitude/latitude coordinates (bottom).

a maximum Courant Number that is as close as possible to, but smaller than 1. Close to the polar regions, the advection step in the longitudinal direction is for Slopes and Second Moment further subdivided. This could also be done for the schemes Split-u, Split-us and Split-rg. Mol-rg and Donorcell are 3D schemes, so the time step Δt_{adv} is restricted by the relation

$$\max_{i,j,k}(\nu_{\lambda_{i,j,k}} + \nu_{\phi_{i,j,k}} + \nu_{\eta_{i,j,k}}) \leq \begin{cases} 1 & \text{(Donorcell)}, \\ \frac{2}{3} & \text{(Mol-rg)}, \end{cases} \tag{3.16}$$

where

$$\begin{aligned} \nu_{\lambda_{i,j,k}} &= \max\left(f_{\lambda_{(i-\frac{1}{2},j,k)}}, f_{\lambda_{(i+\frac{1}{2},j,k)}}\right) \Delta t_{adv} \left(V_{(i,j,k)}\, \rho_{(i,j,k)}\right)^{-1}, \\ \nu_{\phi_{i,j,k}} &= \max\left(f_{\phi_{(i,j-\frac{1}{2},k)}}, f_{\phi_{(i,j+\frac{1}{2},k)}}\right) \Delta t_{adv} \left(V_{(i,j,k)}\, \rho_{(i,j,k)}\right)^{-1}, \\ \nu_{\eta_{i,j,k}} &= \max\left(f_{\eta_{(i,j,k-\frac{1}{2})}}, f_{\eta_{(i,j,k+\frac{1}{2})}}\right) \Delta t_{adv} \left(V_{(i,j,k)}\, \rho_{(i,j,k)}\right)^{-1}. \end{aligned}$$

Numerical tests in [*Hundsdorfer et al.*, 1995] indicate that the underlying 2D version of the Mol-rg scheme is stable and monotonic when applying this restriction on the time step.

4. Problem I: Solid-body rotation on a sphere

4.1 Introduction

The solid-body rotation is a well known test problem for advection schemes [*Williamson and Rasch*, 1989]. In this test we only have horizontal advection, so we solve Equation (3.15) with $f_\eta = 0$. As in [*Smolarkiewicz and Rasch*, 1991; *Hundsdorfer and Spee*, 1995], we consider a cone-shaped initial profile c_0, a cylinder-shaped initial profile c_1 and a smooth initial profile c_2 given by

$$c_0(\lambda,\phi) = \max(0, 1 - r(\lambda,\phi)/R), \tag{4.17a}$$

$$c_1(\lambda,\phi) = \begin{cases} 1 & \text{if } r(\lambda,\phi) > R, \\ 2 & \text{if } r(\lambda,\phi) \leq R, \end{cases} \tag{4.17b}$$

$$c_2(\lambda,\phi) = \cos^4(\lambda - \pi/2)\cos^4(\phi), \tag{4.17c}$$

where

$$r(\lambda,\phi) = 2\sqrt{\left(\cos(\phi)\sin(\tfrac{1}{2}(\lambda - \tfrac{3}{2}\pi))\right)^2 + \left(\sin(\tfrac{1}{2}\phi)\right)^2},$$

and $R = 7\pi/64$. With the smooth profile we can test the convergence behavior, the cylinder profile with background is useful to test whether or not the advection schemes are monotonic, and the cone profile shows the amount of smearing.

The velocities are given by

$$u = 2\pi(\cos\beta\cos\phi + \sin\beta\sin\phi\cos\lambda), \quad v = -2\pi\sin\beta\sin\lambda, \tag{4.18}$$

where $\beta = 90°$. Observe that the wind velocities are constant in time. With this wind field, the exact solution after a full rotation is equal to the initial profile. This wind field is numerical divergent free, if the grid sizes in the λ and ϕ direction are equal, because the divergence of the solid-body wind field is proportional to

$$\begin{aligned} & -v_{out}\cos\phi_{j+\frac{1}{2}} + u_{out} + v_{in}\cos\phi_{j-\frac{1}{2}} - v_{in} \\ = \; & -\sin\beta\sin\lambda_i\cos\phi_{j+\frac{1}{2}} + \cos\beta\cos\phi_j + \sin\beta\sin\phi_j\cos\lambda_{i+\frac{1}{2}} \\ & +\sin\beta\sin\lambda_i\cos\phi_{j-\frac{1}{2}} - (\cos\beta\cos\phi_j + \sin\beta\sin\phi_j\cos\lambda_{i-\frac{1}{2}}) \\ = \; & -\sin\beta\sin\lambda_i(\cos\phi_{j+\frac{1}{2}} - \cos\phi_{j-\frac{1}{2}}) + \sin\beta\sin\phi_j(\cos\lambda_{i+\frac{1}{2}} - \cos\lambda_{i-\frac{1}{2}}) \\ = \; & \sin\beta\sin\lambda_i(2\sin\phi_j\sin\tfrac{\Delta\phi}{2}) - \sin\beta\sin\phi_j(2\sin\lambda_i\sin\tfrac{\Delta\lambda}{2}) \\ = \; & 2\sin\beta\sin\lambda_i\sin\phi_j(\sin\tfrac{\Delta\phi}{2} - \sin\tfrac{\Delta\lambda}{2}). \end{aligned} \tag{4.19}$$

See Figure 2 for the definition of v_{out}, u_{out}, v_{in} and u_{in}. We used the equality

$$\cos(x + dx) - \cos(x - dx) = -2\sin(x)\sin(dx).$$

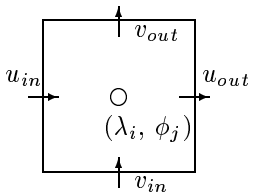

Figure 2: In and outgoing velocities.

coarse grid: $N_\lambda \times N_\phi = 64 \times 33$; $\Delta_\lambda = \Delta_\phi = 5.625° \approx 5.6°$

scheme	CPU	nt	$\frac{\text{CPU}}{\text{nt}\, N_\lambda\, N_\phi}$	undershoot	overshoot	smearing	L2
	s		ms	EMIN c_1	EMAX c_1	EMAX c_0	ERR0 c_2
Second M.	1.8	82	10.5	-2.26E-2	1.50E-2	-1.71E-1	1.55E-2
Slopes	0.7	82	4.0	-1.89E-2	4.16E-2	-2.57E-1	1.42E-2
Split-u	1.8	163	5.2	-1.45E-13	-3.29E-2	-4.72E-1	8.61E-3
Split-us	0.4	48	4.0	-2.71E-13	-2.59E-3	-3.77E-1	6.22E-3
Split-rg	0.7	78	4.5	4.32E-14	-9.09E-2	-5.73E-1	1.67E-2
Mol-rg	1.2	263	1.1	-2.82E-14	-1.42E-1	-6.48E-1	2.07E-2
Donorcell	0.2	174	0.4	1.90E-7	-3.77E-1	-9.00E-1	1.48E-1

middle grid: $N_\lambda \times N_\phi = 128 \times 65$; $\Delta_\lambda = \Delta_\phi = 2.8125° \approx 2.8°$

scheme	CPU	nt	$\frac{\text{CPU}}{\text{nt}\, N_\lambda\, N_\phi}$	undershoot	overshoot	smearing	L2
	s		ms	EMIN c_1	EMAX c_1	EMAX c_0	ERR0 c_2
Second M.	37.7	326	13.9	-3.36E-2	3.65E-2	-9.05E-2	5.45E-3
Slopes	10.5	326	3.9	-2.14E-2	3.89E-2	-1.37E-1	4.86E-3
Split-u	29.4	652	5.4	-1.15E-12	-2.26E-6	-2.22E-1	1.61E-3
Split-us	3.1	96	3.9	-6.71E-13	-2.56E-9	-1.66E-1	1.35E-3
Split-rg	3.8	108	4.2	-1.44E-13	-8.65E-5	-2.82E-1	3.16E-3
Mol-rg	6.8	415	2.0	-1.36E-16	-6.50E-3	-3.75E-1	4.06E-3
Donorcell	1.2	274	0.5	2.00E-15	-2.72E-1	-8.13E-1	8.53E-2

finest grid: $N_\lambda \times N_\phi = 256 \times 129$; $\Delta_\lambda = \Delta_\phi = 1.40625° \approx 1.4°$

scheme	CPU	nt	$\frac{\text{CPU}}{\text{nt}\, N_\lambda\, N_\phi}$	undershoot	overshoot	smearing	L2
	s		ms	EMIN c_1	EMAX c_1	EMAX c_0	ERR0 c_2
Second M.	3039	1304	70.6	-3.17E-2	3.63E-2	-4.61E-2	1.91E-3
Slopes	351	1304	8.2	-2.93E-2	3.54E-2	-7.90E-2	1.69E-3
Split-u	671	2608	7.8	-4.64E-12	1.64E-14	-1.17E-1	3.38E-4
Split-us	36	192	5.7	-2.77E-12	7.31E-14	-9.29E-2	3.31E-4
Split-rg	60	325	5.6	-6.49E-13	-6.88E-11	-1.50E-1	6.52E-4
Mol-rg	115	993	3.5	-2.10E-13	-1.07E-8	-1.65E-1	7.32E-4
Donorcell	31	724	1.3	-6.84E-14	-1.65E-1	-6.97E-1	5.51E-2

Table 1: Results for solid-body rotation test on a sphere.

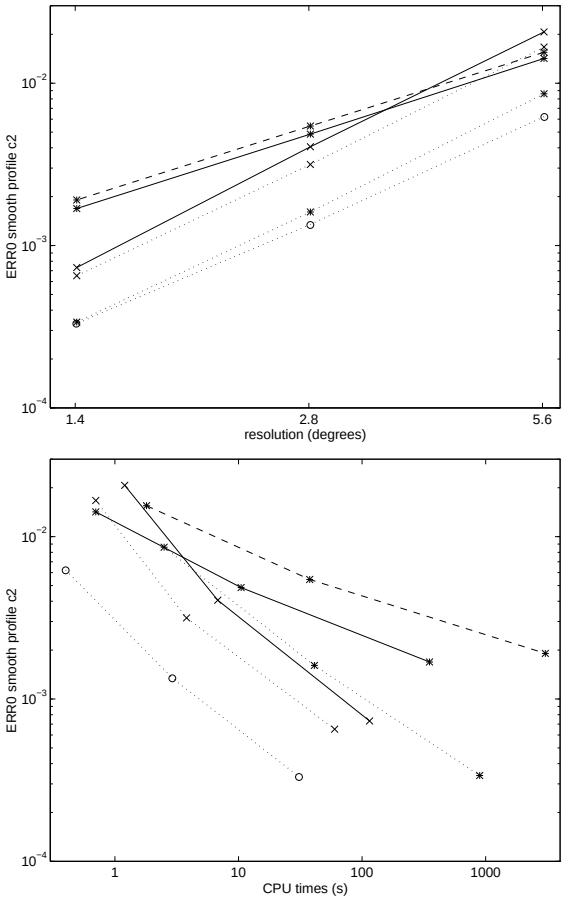

Figure 3: Convergence behavior. Bottom: L2 as a function of CPU time, top: L2 as a function of the resolution. *-solid: Slopes, *-dashed: Second Moment, *-dotted: Split-u, o-dotted: Split-us, x-dotted: Split-rg, x-solid: Mol-rg. Results for Donorcell fall outside these plots.

4.2 Results for problem I

The results for the solid-body rotation test are given in Table 1. We use the same errors as *Smolarkiewicz and Rasch* [1991], defined by

$$\text{EMIN} = \frac{\min(c^n_{i,j}) - \min(c_{i,j}(t_n))}{\max(c_{i,j}(t_n))}, \qquad \text{EMAX} = \frac{\max(c^n_{i,j}) - \max(c_{i,j}(t_n))}{\max(c_{i,j}(t_n))},$$

$$\text{ERR0} = \frac{(\sum \gamma_j (c^n_{i,j} - c_{i,j}(t_n))^2)^{1/2}}{\max(c_{i,j}(t_n))},$$

where $\gamma_j = \cos(\phi_j)/(N_\lambda \sum_{k=1}^{N_\phi} \cos(\phi_k))$. The scaling is chosen such that ERR0 will be equal to 1 if the error is 1 in all grid points and $\max(c_{i,j}(t_n)) = 1$. The sums and max/min values are taken over $i = 1, \cdots, N_\lambda,\ j = 1, \cdots, N_\phi$. In all formulas $c_{i,j}(t_n)$ denotes the reference solution, and $c^n_{i,j}$ the computed solution at time t_n, the time necessary for a full rotation. The number of steps necessary to fulfill the CFL condition for a full rotation is nt. Small typed numbers are close to round-off.

The smearing is given by the EMAX with the cone c_0 as initial profile and L2 is the ERR0 error for the smooth initial profile c_2. We define overshoot as the EMAX error and undershoot as the EMIN error, both with the cylinder c_1 as initial profile.

The EMAX error with the cylinder c_1 is influenced by overshoot and numerical diffusion. The influence of numerical diffusion decreases with increasing resolution. In this test we see that for the new schemes this error is purely caused by numerical diffusion, and not by overshoot, so we conclude that these schemes are monotonic. The limiter used in Slopes and Second Moment prevents only negative values, resulting in 3 percent overshoot and undershoot.

The Split-us scheme gives very good results for this test. This may not be the case in a full scale transport chemistry model, because the time step can be determined by other processes, so that Split-us must take smaller time steps than necessary from a point of stability. The timing is done on a workstation and we know that on a vector processor such as the Cray C90, the efficiency for the flux calculation in the longitudinal direction is low. This is caused by the summation over c_l in Equations (12) and (13) in [*Hundsdorfer and Spee*, 1995]. The difference between L2 for uniform and reduced grid is quite large, which is caused by the fact that in this test the centre of the transported concentrations is relatively long in the polar regions. If in actual computations the polar regions are of special interest, one could start grid reduction at e.g. 70° instead of 60°. Note that also Split-rg can be made unconditionally stable, with as disadvantage a low efficiency on a vector processor.

Differences in CPU time are mainly caused by nt. For Split-us and the schemes on a reduced grid a doubling of the resolution leads to a doubling of nt, whereas on a uniform grid nt quadruples for explicit finite volume schemes, due to the extra factor 2 coming from the $\cos\phi$. So on high resolutions, a reduced grid or unconditional stability is necessary to avoid very small time steps. We prefer the reduced grid approach, because all other processes need about 25 percent less CPU due to the lower number of cells. Other differences in CPU are caused by the number of flux calculations per step (7 for Slopes, Second Moment and Split-u, 6 for Mol-rg, 5 for Split-us and Split-rg, and 3 for Donorcell), and the costs of one flux calculation, which is relatively high for limited schemes. Timings also depend on implementation, of coarse.

Slopes and Second Moment need respectively 4 to 10 times more memory, due to the storage of the first and second order moments of the transported species. This will hardly change when using Second Moment on a reduced grid, as in [*Prather et al.*, 1987]. In our hardware configuration, this gives problems with the data-cache, which is the reason why the ratio CPU / (nt $N_\lambda\, N_\phi$) is not constant for a given method when increasing the resolution.

We observe that Split-us, Split-rg and Mol-rg give good results for smooth profiles and therefore good convergence speed, see Figure 3. Also with block profiles the new schemes give good results. Slopes and Second Moment give good results for the cone tests.

In [*Hundsdorfer and Spee*, 1995] we compared the dimensional splitting schemes with the semi-Lagrangian TREMBA schemes used in [*Smolarkiewicz and Rasch*, 1991], and concluded that our schemes are more accurate than the the second-order method, but slightly less accurate than the

nonlimited TREMBA schemes of orders 4 and 6. We know that the unlimited version of our schemes are more accurate, but we focus on mass conservative and monotonic schemes.

We conclude that Split-u and Second Moment are too expensive. Results for Split-u will therefore not be given in the radon test, but results for Second Moment are given for reasons of comparison.

5. Problem II: Radon test

5.1 Introduction

We assume that the radioactive noble gas radon-222 (^{222}Rn) is emitted with a constant flux of 1 atom $cm^{-2}\,s^{-1}$ from land surface and no flux from the ocean. *Heimann et al.* [1990] observes that the value of 1 atom $cm^{-2}\,s^{-1}$ is uncertain to almost a factor of two, and the flux from the ocean is two to three orders of magnitude smaller, so we can neglect the contribution from the ocean. When the land is covered with a permafrost layer or snow the emission flux is zero. For January we use the climatological value of 60°N, taken from ECHAM, for the latitude circle that bounds the area covered with permafrost or snow layers. The half-life of ^{222}Rn is 3.8 days. We use ^{222}Rn to perform a horizontal transport experiment that discriminates between the different advection schemes under real atmospheric conditions.

Two datasets of KNMI-preprocessed ECMWF operational intialized analyses for the month January 1992 are used as input to the 3D chemical transport model. Pressure level fields from ECMWF's operational archive with a vertical resolution of 15 layers and transformed to a uniform 2.5°× 2.5° grid were used as input to the preprocessing procedure. The time resolution of both preprocessed datasets is 12 hours, the spatial resolution is respectively 5.0°× 3.8° and 2.5°× 2.5° in the horizontal and 15 layers in the vertical direction [*Velders et al.*, 1994]. The datasets contain the grid-resolved mass fluxes and the input necessary to calculate sub-grid scale vertical transport. The preprocessing routines for the TM2 model [*Heimann*, 1995] were used in constructing these data.

The differences between the different advection schemes become apparent in differences between maximum surface concentrations (for instantaneous fields this could be up to a 5% difference), 'plume-around-maximum' areas, surface concentration front patterns near coastlines, and the structure of 'radon concentration peaks' associated with rapid advection of boundary-layer air from continents to remote oceanic sites. Numerical diffusion and numerical dispersion are critical concerns in the simulation of oceanic radon concentration patterns [*Brost and Chatfield*, 1989; *Balkanski and Jacob*, 1990]. In the world's oceans there are only three remote island sites where the surface ^{222}Rn concentration is continuously measured: Amsterdam Island (77°34'E, 37°50'S), Crozet Island (51°52'E, 46°26'S), and Kerguelen (70°15'E, 49°21'S), all on French territory. These datasets are maintained and updated by the Centre de Faibles Radioactivités (CFR) and the Laboratoire de Modélisation du Climat et de l'Environnement (LMCE). We use the data of these three islands, see Figure 4, for January 1992 in order to compare the different numerical simulations with actual measurements.

5.2 Results for the radon test

From the comparison between measurements and numerical model calculations, plotted in Figure 5, we can see that for both resolutions the model does not show a systematic bias in the predicted concentrations. *Heimann et al.* [1990] found too high model concentrations at all stations using ECMWF wind fields at a resolution of 10.0° × 7.8° and the Slopes scheme, while *Balkanski and Jacob* [1990] using GISS GCM wind fields at a resolution of 5.0° × 3.8° and the Second Moment scheme did not simulate such a bias.

Note that we compare the model results with the measurements only for the last 18 days, because the model results for the first two weeks strongly depend on the initial concentration used.

In Figures 6 and 7 model results at the two resolutions are plotted. For all stations and all resolutions the strong diffusivity of the Donorcell scheme causes significantly higher background concentrations over the oceans than as simulated with the other, less diffusive, numerical schemes. However, even the Donorcell scheme does not systematically overpredict the concentrations. The similar background concentrations simulated by the Slopes scheme and the Second Moment scheme (the last one is not

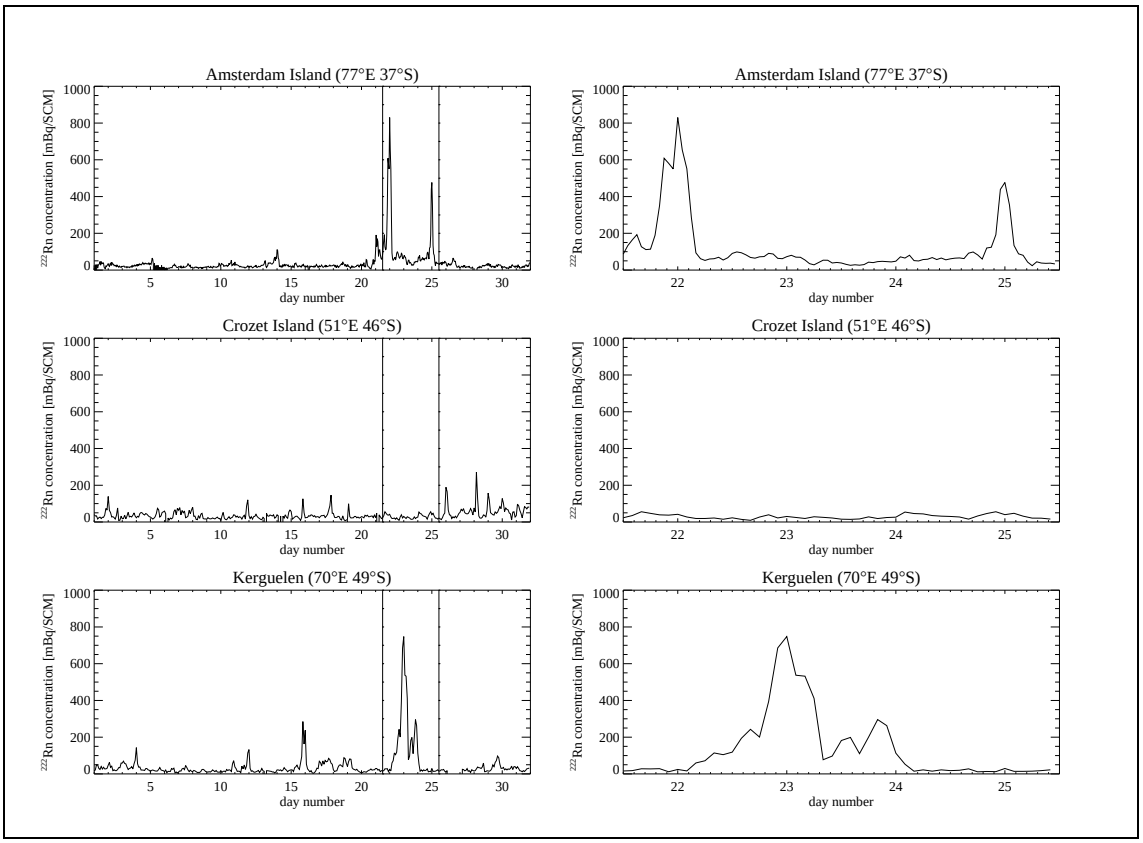

Figure 4: Measured radon concentrations at three islands in the Indian Ocean in January 1992. The day numbers correspond to the time 0000 UTC at the respective days of the year 1992. On the right hand side the period from 1200 UTC January 21 1992 to 1200 UTC January 25 1992 has been magnified.

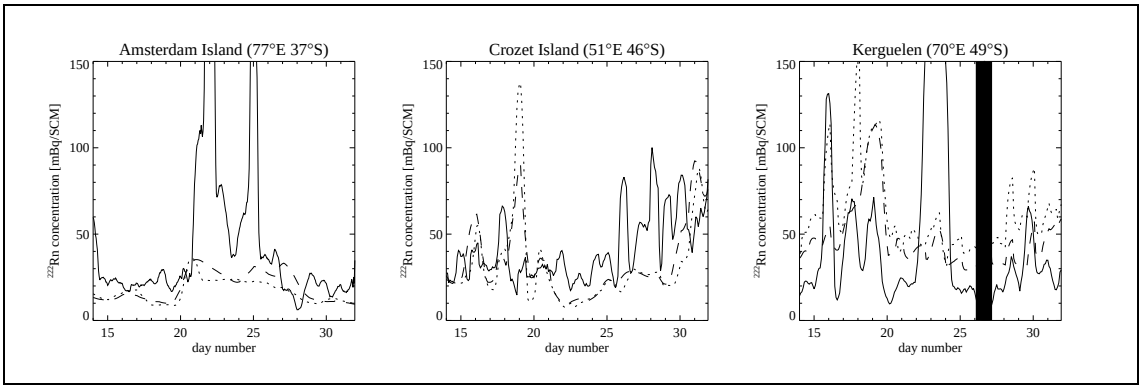

Figure 5: Smoothed local radon concentration measurements (solid line) and numerical model results at two resolutions, respectively $2.5° \times 2.5°$ (dotted) and $5.0° \times 3.8°$ (dashed), from 0000 UTC 14 January 1992 to 2400 UTC 31 January 1992. The numerical scheme in this plot is the Split-rg scheme. The lowest model grid cell that is nearest to the measurement points is used. For Kerguelen the black bar indicates that measurements are not available from 0000 UTC 26 January 1992 to 0600 UTC 27 January 1992.

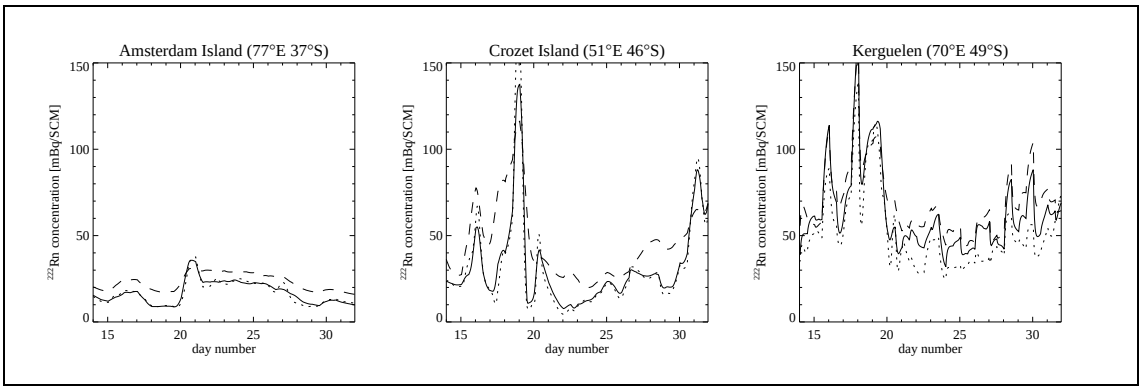

Figure 6: Numerical model results at a resolution of $2.5° \times 2.5°$ for different numerical schemes from 0000 UTC 14 January 1992 to 2400 UTC 31 January 1992. Results are plotted for the Split-rg (solid line), Slopes (dotted), and Donorcell (dashed) schemes. The lowest model grid cell that is nearest to the measurement points is used.

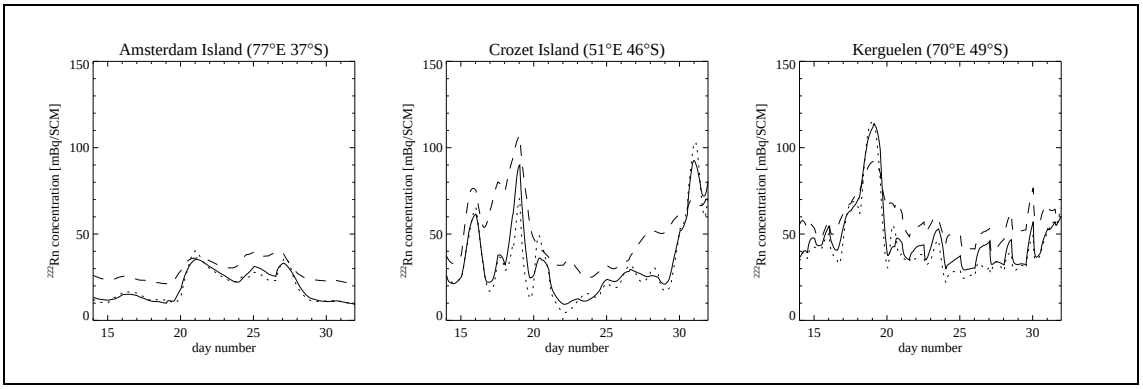

Figure 7: Numerical model results at a resolution of $5.0° \times 3.8°$ for different numerical schemes. Same plot as Figure 6.

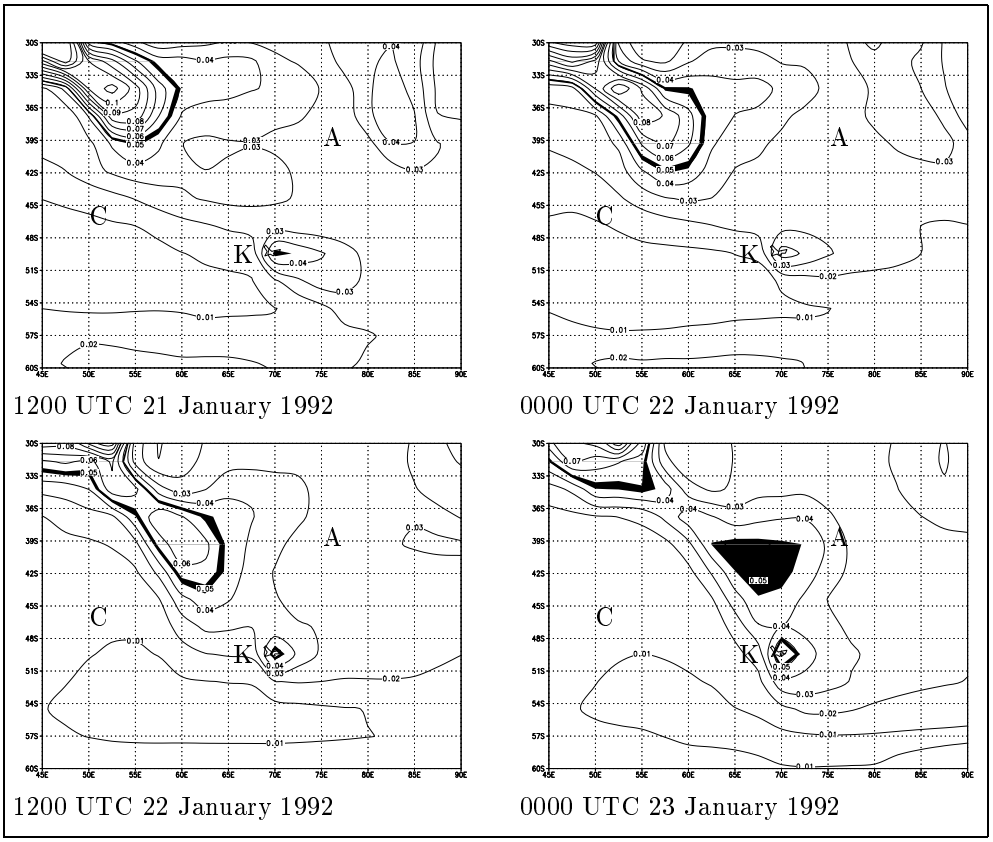

Figure 8: Contourlines of ^{222}Rn in Bq/SCM in a part of the Indian Ocean. A, C and K indicates the location of Amsterdam Island, Crozet Island and Kerguelen respectively. Results are obtained with Second Moment. We use black shading for values between 48 and 52 mBq/SCM.

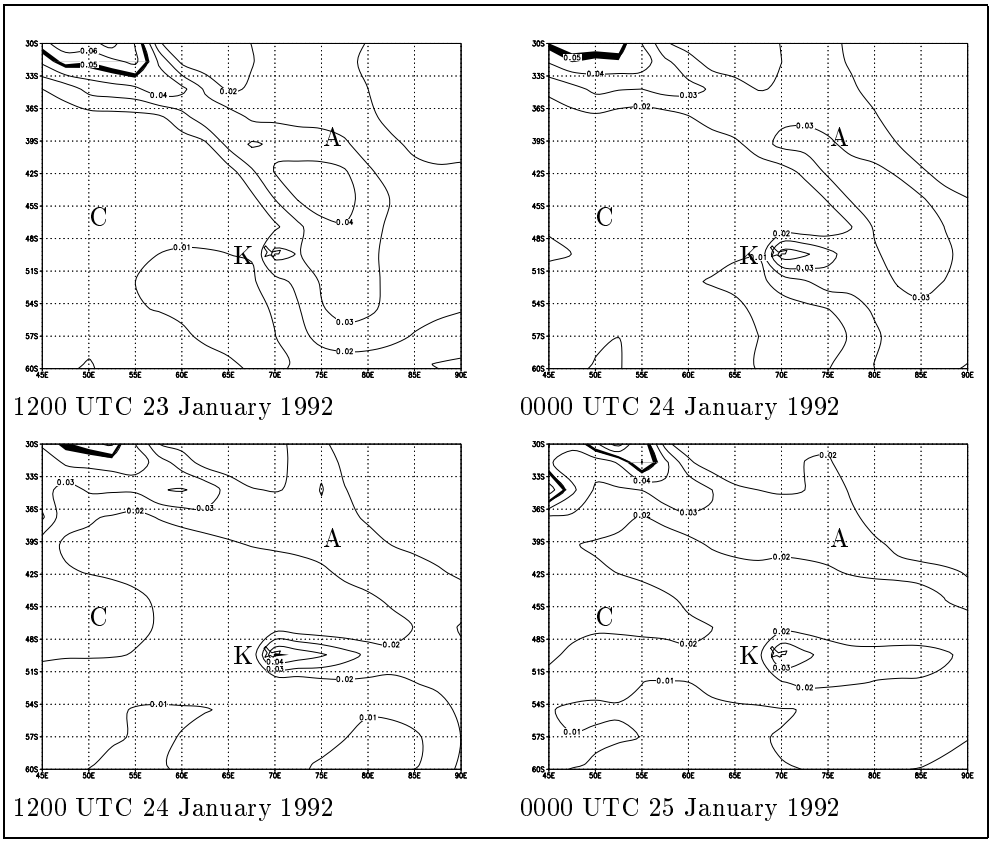

Figure 9: As Figure 8, next 2 days.

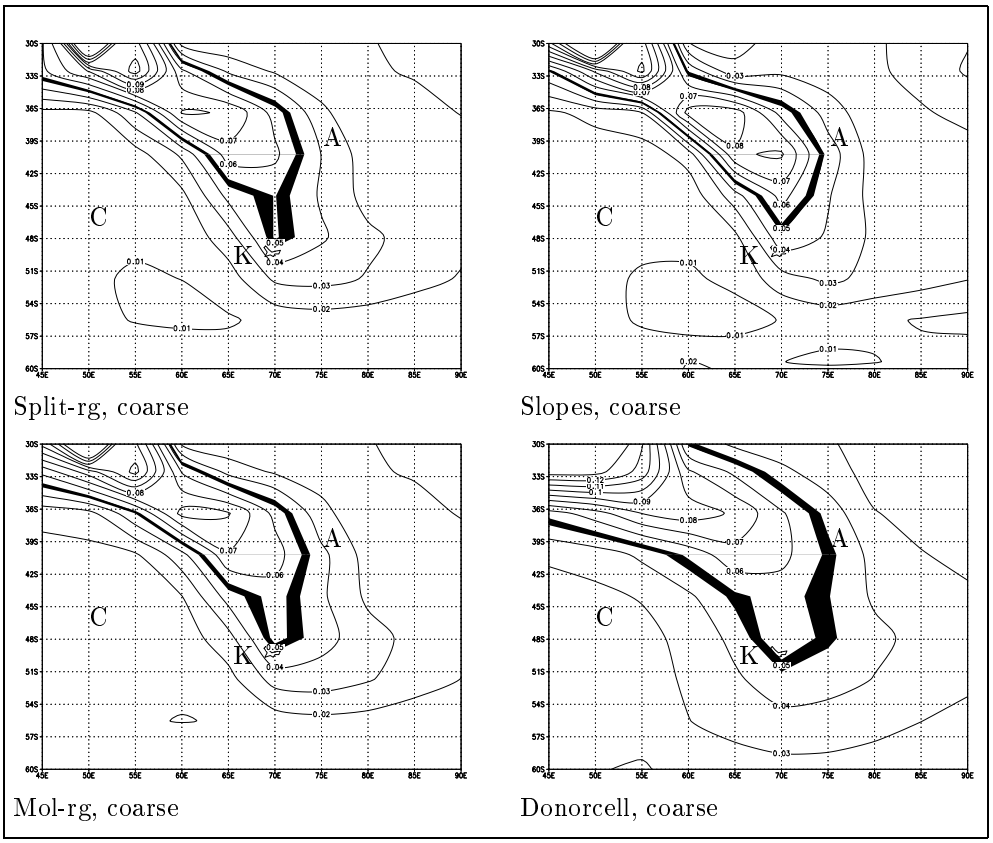

Figure 10: The same plot as Figure 8, but now for different advection schemes and the coarse resolution at 0000 UTC 23 January 1992.

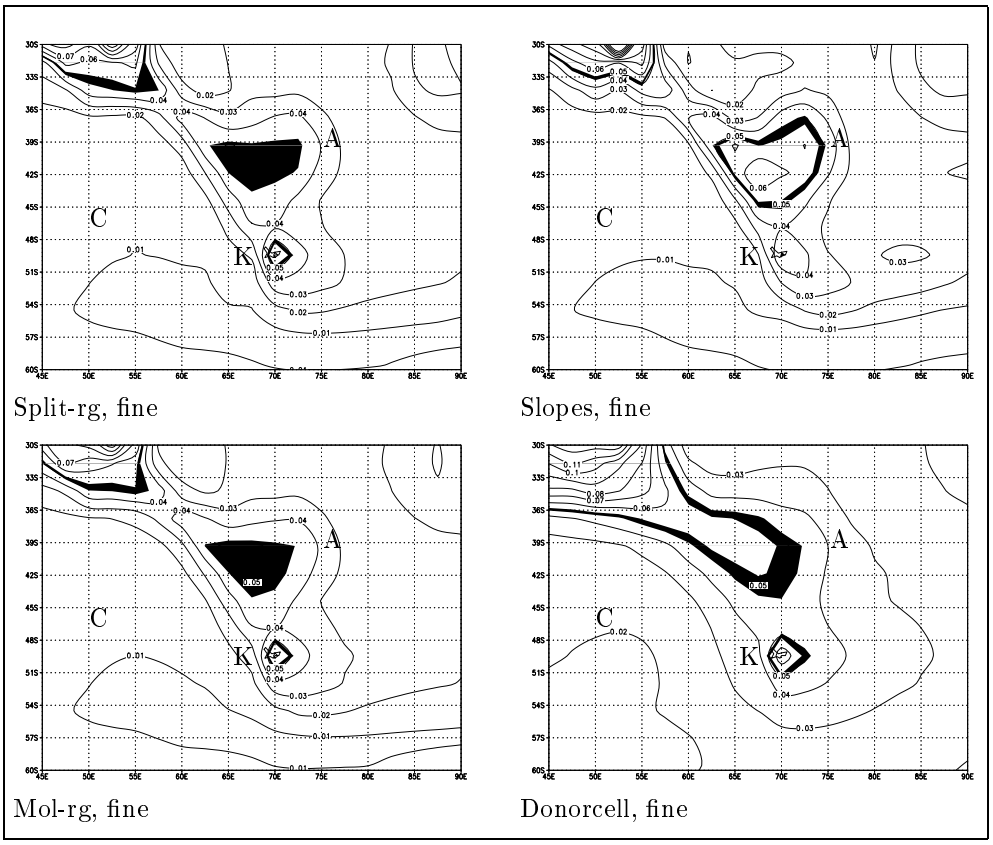

Figure 11: Same plot as Figure 10, but now fine resolution.

shown) confirm the suggestion in [*Heimann et al.*, 1990] that the difference between their model results and those of in [*Balkanski and Jacob*, 1990] are mainly due to differences in resolution and not in numerical schemes. The results for the Split-us scheme coincide with the results for the Split-rg scheme, and are therefore not shown.

From Figure 5 it can be concluded that the correlation between measured and simulated peaks of radon concentrations is poor for this 18-day period. For Amsterdam Island the measured radon concentration peaks at 21/22 January and 24/25 January do not appear in the model. For Crozet Island no radon concentration peaks were measured while the model simulates a radon concentration peak at 18 January. For Kerguelen two radon concentration peaks were measured, one at 15 January (also simulated in the model) and one at 22/23 January (not simulated). The model simulates two additional radon concentration peaks at 17/18 and 19 January which coincide with much weaker peaks in the measurements. In Figures 8 and 9 the radon concentration fields are shown for the 4-day period from 1200 UTC 21 January 1992 to 0000 UTC 25 January 1992 (measurements also shown separately in Figure 4). Note that the area of Kerguelen is quite large and hence we have significant radon emission on Kerguelen itself. From 1200 UTC 21 January 1992 to 0000 UTC 23 January 1992 we can see that the 50 mBq/SCM isopleth moves in south-east direction between Amsterdam and Crozet Islands, while it diminishes in size. However, as described before, measurements at Amsterdam Island show a peak higher than 150 mBq/SCM at 21/22 January, and measurements at Crozet Island show no peak. Shortly after the measured peak passed Amsterdam Island it passed Kerguelen. In the model simulation the peak has diminished its strength before it reaches Kerguelen. Near the end of the 4-day period, shown in Figure 9, the radon concentrations start to increase again a little in the upper left hand corner of the shown domain and at Crozet and Amsterdam Islands. However, this small increase remains far below the radon peak concentrations above 150 mBq/SCM measured at Amsterdam Island on 25 January.

Here we summarize the performance of the model in simulating the radon concentration peaks at Amsterdam Island. At 22/23 January the simulated radon concentration peak between Amsterdam and Crozet Islands is simulated (i) approximately 750 km too much to the west, (ii) 1 day too late, and (iii) a factor 3 too low. At 25 January a similar radon peak as on 21/22 was measured at Amsterdam Island, but in the model a much weaker peak did not reach a position closer than approximately 1000 km to the west-north-west of the island.

Two causes for the transport model errors can be identified. One is the error in the lower tropospheric circulation pattern as analyzed by ECMWF. This is due to a lack of meteorological measurements in the Southern Indian Ocean region that can be used in the data assimilation procedure at ECMWF. Another source of errors is the use of a 12-hour time resolution of the input meteorology instead of using a higher time resolution, for example by doing on-line tracer transport in a climate or weather forecast model nudged towards observed meteorology.

In Figure 12 we show the wind directions calculated from the model input (ECMWF analyses) compared to the observed wind directions at the three islands for the month January 1992. In the specific period that we focus on in this paper (21 January 1992 to 25 January 1992) we can conclude from Figure 12 that in reality the wind was more directed in the west-to-east direction compared to the ECMWF analyses used in our model. This is consistent with the fact that the plume simulated at 22/23 January 1992 was too much to the west. Using a higher time resolution in a climate model nudged towards the ECMWF analyses, would probably have produced a similar erroneous result. However, from this limited period no general conclusions regarding the respective contributions of both error sources can be drawn.

To evaluate the general capability of the model to simulate radon concentration peaks (looking now at their structure and not their timing) we compared autocorrelation functions for both model resolutions with the autocorrelation function for the 12-hourly smoothed measurements (not shown). Although an 18-day period is too short to formulate firm conclusions about radon concentration peak statistics, we find that for the $2.5^\circ \times 2.5^\circ$ resolution the autocorrelation functions generally fall off to 0.5 at a similar time lag of approximately 15 hours as for the smoothed data. In [*Heimann et al.*,

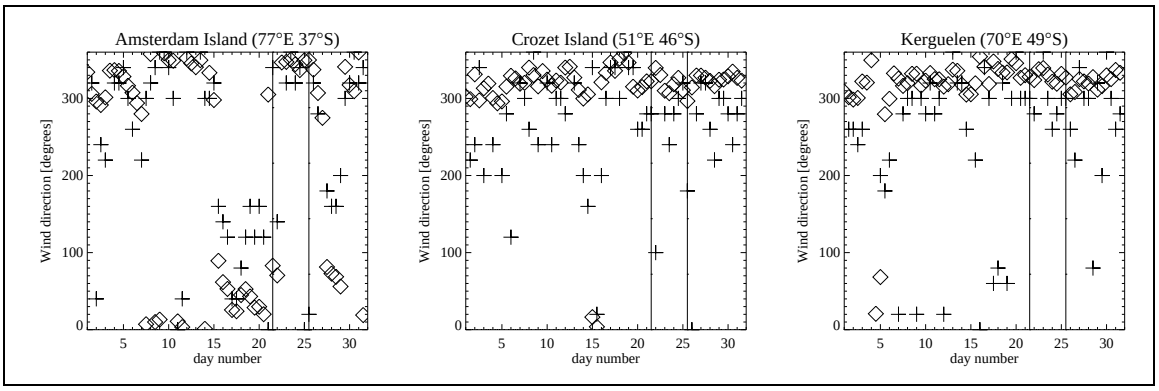

Figure 12: Measured wind directions (crosses) and wind directions calculated from ECMWF initialized analyses (diamonds), both plotted at 12-hour time resolution. A wind direction of zero degrees corresponds to north-to-south. The period from 1200 UTC 21 January 1992 to 1200 UTC 25 January 1992 is indicated in the plots.

1990], using a whole year in the calculation of the autocorrelation, the time lag at an autocorrelation of 0.5 was found to be twice as large in their model as in their smoothed data. We find the same difference between our $5.0° \times 3.8°$ resolution results and the data, indicating that a spatial resolution of $2.5° \times 2.5°$ is needed to adequately represent time scales of the order of 12 hours in atmospheric transport models. This conclusion is related to the flow structure in the lower troposphere and is independent of numerics.

In Figures 10 and 11 we give isopleths for four advection schemes for coarse and fine resolution respectively. As expected, the results for the Donorcell algorithm differ strongly from all other schemes. Also the difference between both resolutions is remarkable. Split-rg and Split-us give identical results, and the difference with the results from Second Moment (given in Figure 8) and Slopes is small.

The main purpose of this radon test for horizontal transport is to compare the performance of different numerical advection schemes under more realistic meteorological conditions. We have found that the numerical accuracy of Slopes, Second Moment and the four newly developed schemes is comparable for these conditions. In future studies on radon transport longer time integrations and a comparison between on-line and off-line transport model results will have to be performed. The influence of different numerical advection schemes on the results will be very small, therefore the most efficient advection scheme can be used.

5.3 Performance results

In Table 2 results are given from a performance test, for a simulation of one month on the $2.5° \times 2.5°$ grid. We give results for the subroutines `do_conv`, `calc_conv` and `advection`. They respectively solve Equation (2.8), the sub-grid scale vertical transport parametrization, Equation (2.10), the calculation of the convection matrix and the advection equation. The CPU time is in minutes on a workstation.

The time step for advection, Δt_{adv}, was always 30 minutes for the dimensional splitting schemes on the coarse grid, and depending on the actual wind velocities 15 or 30 minutes on the fine grid. The time step for Mol-rg and Donorcell was 10, 15 or 30 minutes.

We see that on a reduced grid 15 % CPU is saved in `calc_conv`, and `do_conv` becomes expensive when using Slopes or Second Moment: it consumes more CPU time than Split-rg needs for advection. In a model with several chemical species the calculations in `do_conv` and `advection` must be done for all species involved, so it is important that these calculations are performed very efficiently.

From the radon test we know that the differences between Split-us, Split-rg, Mol-rg, Slopes and

method	do_conv	calc_conv	advection	total
Donorcell	11	4	10	26
Split-rg	10	4	18	33
Split-us	14	5	22	41
Mol-rg	11	4	41	57
Slopes	24	5	60	90
Second M.	52	5	147	205

Table 2: CPU times in minutes for a simulation of one month for some parts of the transport model.

Second Moment are very small, but from the results in Table 2 we see that Split-us and Split-rg are by far the most efficient solvers for pure advection, and all solvers on a reduced grid are 1.3 times faster in solving the sub-grid scale vertical transport parametrization than Split-us, three times faster than Slopes, and five times faster than Second Moment.

We conclude that Split-us and Split-rg are the most efficient solvers for this application, but in models with complicated chemistry the reduced grid is recommended, because the chemistry is solved 1.3 times faster and the efficiency on a vector processor of Split-us is lower.

6. Conclusion

We have presented four new advection schemes, especially designed for advection of trace gases in global air quality models. Important characteristics of these schemes are that they are mass conservative and that they do not generate undershoot and overshoot. Mass conservation is important because long-term calculations are performed with these models and the generation of undershoot may introduce negative values, possible resulting in instability when combined with stiff chemistry. The schemes should be very efficient on (parallel) vector processors in terms of CPU time, memory requirements and accuracy. Also the pole singularity must be solved.

We performed two tests: a solid-body rotation test, where we can compare numerical results with an exact solution and a radon test where we compare model results with measurements. The new schemes are compared with two advection solvers that are currently widely used in global transport models: Slopes and Second Moment.

From the solid-body rotation test we learn that all new schemes do not generate undershoot and overshoot, and are mass conservative. Split-us and Split-rg give accurate results and are very cheap in terms of CPU time and memory requirements. The schemes on a reduced grid, Split-rg and Mol-rg, and Split-us give good convergence speed, an important property when increasing the resolution. Unfortunately, Split-us is not very efficient on a vector processor.

For the radon test, difference between advection schemes are minor for the grid resolutions used. From a comparison with the measurements we can furthermore conclude that the difference between results for different spatial resolution is much smaller than the difference between the model and the measurements. Errors in the lower tropospheric flow patterns, due to a lack of meteorological measurements, as analyzed by the ECMWF for the month January 1992 in the Southern Indian Ocean region and errors related to the low time resolution of the input meteorology must be considered as the main sources of difference between the transport model and the measurements.

Slopes and Second Moment need a lot of CPU time in handling the moments during convection. They would have the same problem when chemistry is added to the model. The memory requirements for these schemes are respectively 4 and 10 times larger than for the other schemes.

At higher spatial resolutions the pole problem becomes more apparent. We have presented two options to overcome this difficulty: the reduced grid and the unconditionally stable Split-us scheme on a uniform grid. We generally recommend the use of Split-rg on a reduced grid because it has 25 percent less cells for the same spatial resolution at moderate latitudes, while good efficiency on a

vector processor, such as the Cray C90, is obtained.

From both tests we conclude that Split-rg gives almost the same model results as Slopes and Second Moment for significant less CPU time and memory requirements. Therefore we recommend Split-rg for solving the advection equation in global air quality models.

Acknowledgements A.C. Petersen acknowledges the facilities offered by the Royal Netherlands Meteorological Institute (KNMI), partner in the Netherlands Centre for Climate Research (CKO), during his stay at KNMI. Drs. P.F.J. van Velthoven (KNMI), B.J.J.M. van den Hurk (KNMI) and Y.J. Balkanski (CFR) provided the preprocessed meteorological data, the wind observations and radon measurements, respectively. Dr. F.J. Dentener (IMAU) has given useful comments on a previous version of the manuscript. A.C. Petersen acknowledges support by the Netherlands Geosciences Foundation (GOA) with financial aid from the Netherlands Organization for Scientific Research (NWO). E.J. Spee and W. Hundsdorfer gratefully acknowledge financial support from the Dutch National Institute of Public Health and Environmental Protection (RIVM) for the research project CIRK.

References

Allen, D.J., A.R. Douglas, R.B. Rood, and P.D. Guthrie. Application of a monotonic upstream-biased transport scheme to three-dimensional constituent transport calculations. *Mon. Wea. Rev.*, 119:2456–2464, 1991.

Balkanski, Y.J., and D.J. Jacob. Transport of continental air to the subantarctic Indian Ocean. *Tellus*, 42B:62–75, 1990.

Blom, J.G., W. Hundsdorfer, and J.G. Verwer. Vectorization aspects of a spherical advection scheme on a reduced grid. Technical Report NM-R9418, CWI, Amsterdam, 1994.

Bott, A. Monotone flux limitation in the area-preserving flux-form advection algorithm. *Mon. Wea. Rev.*, 120:2595–2602, 1992.

Brost, R.A., and R.B. Chatfield. Transport of radon in a three-dimensional, subhemispheric model. *J. Geophys. Res.*, 94:5095–5119, 1989.

Chin, M., D.J. Jacob, G.M. Gardner, M.S. Foreman-Fowler, and P.A. Spiro. A global three-dimensional model of tropospheric sulfate. *J. Geophys. Res.*, 101:18667–18690, 1996.

Crutzen, P.J., and P.H. Zimmermann. The changing photochemistry of the troposphere. *Tellus*, 43:136–151, 1991.

Easter, R.C. Two modified versions of Bott's positive-definite numerical advection scheme. *Mon. Wea. Rev.*, 121:297–304, 1992.

Feichter, J.E., E. Kjellström, H. Rohde, F.J. Dentener, J. Lelieveld, and G.-J. Roelofs. Simulation of the tropospheric sulfur cycle in a global climate model. *Atmos. Environ.*, 30:1693–1708, 1996.

Heimann, M. The global atmospheric tracer model TM2. Technical Report 10, Deutches Klimarechnenzentrum (DKRZ), Hamburg, Germany, 1995.

Heimann, M., P. Monfray, and G. Polian. Modeling the long-range transport of ^{222}Rn to subantarctic and antarctic areas. *Tellus*, 42B:83–99, 1990.

Hundsdorfer, W., B. Koren, M. van Loon, and J.G. Verwer. A positive finite-difference advection scheme. *J. Comput. Phys.*, 117:35–46, 1995.

Hundsdorfer, W., and E.J. Spee. An efficient horizontal advection scheme for modeling of global transport of constituents. *Mon. Wea. Rev.*, 123:3554–3564, 1995.

Hundsdorfer, W., and R.A. Trompert. Method of lines and direct discretization: a comparison for linear advection. *Appl. Num. Math.*, 13:469–490, 1994.

Koren, B. A robust upwind discretization method for advection, diffusion and source terms. In C.B. Vreugdenhil and B. Koren, editors, *Numerical Methods for Advection-Diffusion Problems*, Notes on Numerical Fluid Mechanics 45, pages 117–138, Braunschweig, 1993. Vieweg.

Louis, J.-F. A parametric model of vertical eddy fluxes in the atmosphere. *Bound.-Layer Meteor.*, 17:187–202, 1979.

Müller, J.-F., and G. Brasseur. IMAGES: A three-dimensional chemical transport model of the global troposphere. *J. Geophys. Res.*, 100:16445–16490, 1995.

Peters, L.K., C.M. Berkowitz, G.R. Carmichael, R.C. Easter, G. Fairweather, S.J. Ghan, J.M. Hales, L.R. Leung, W.R. Pennell, F.A. Potra, R.D. Saylor, and T.T. Tsang. The current state and future directions of Eulerian models in simulating the tropospheric chemistry and transport of trace species: a review. *Atmos. Environ.*, 29:189–222, 1995.

Prather, M.J. Numerical advection by conservation of second-order moments. *J. Geophys. Res.*, 91:6671–6681, 1986.

Prather, M.J., M.B. McElroy, S.C. Wofsy, G. L. Russell, and D. Rind. Chemistry of the global troposphere: Fluorocarbons as tracers of air motion. *J. Geophys. Res.*, 92:6579–6613, 1987.

Rasch, P.J. Conservative shape-preserving two-dimensional transport on a spherical reduced grid. *Mon. Wea. Rev.*, 122:1337–1350, 1994.

Roelofs, G.-J., and J. Lelieveld. Distribution and budget of O_3 in the troposphere calculated with a chemistry general circulation model. *J. Geophys. Res.*, 100:20983–20998, 1995.

Russell, G.L., and J.A. Lerner. A new finite-differencing scheme for the tracer transport equation. *J. Appl. Meteor.*, 20:1483–1498, 1981.

Smolarkiewicz, P.K., and P.J. Rasch. Monotone advection on the sphere: an Eulerian versus semi-Lagrangian approach. *J. Atmos. Sci.*, 48:793–810, 1991.

Spee, E.J. Coupling advection and chemical kinetics in a global atmospheric test model. In H. Power, N. Moussiopoulos, and C.A. Brebbia, editors, *Air Pollution III, Volume 1: Air Pollution, Theory and Simulation*, pages 319–326. Computational Mechanics Publications, Southampton, Boston, 1995.

Strang, G. On the construction and comparison of difference schemes. *SIAM J. Numer. Anal.*, 5:506–517, 1968.

Tiedtke, M. A comprehensive mass flux scheme for cumulus parametrization in large-scale models. *Mon. Wea. Rev.*, 117:1779–1800, 1989.

van Leer, B. Towards the ultimate conservative difference scheme IV, a new approach to numerical convection. *J. Comput. Phys.*, 23:276–299, 1977.

Velders, G.J.M., L.C. Heijboer, and H. Kelder. The simulation of the transport of aircraft emissions by a three-dimensional global model. *Ann. Geophys.*, 12:385–393, 1994.

Williamson, D.L. Review of numerical approaches for modeling global transport. In H. van Dop and G. Kallos, editors, *Air Pollution Modeling and Its Application IX*, pages 377–394. NATO Challenges of Modern Society 17, Plenum Press, New York, 1992.

Williamson, D.L., and P.J. Rasch. Two-dimensional semi-lagrangian transport with shape-preserving interpolation. *Mon. Wea. Rev.*, 117:102–129, 1989.

A. Dimensional splitting in conservation form with mixing ratio fluxes

The new schemes presented and tested in this paper are 3D extensions of earlier derived schemes, such as Split-DeCo in [*Hundsdorfer and Spee*, 1995], and the MOL schemes in [*Hundsdorfer et al.*, 1995]. These schemes are based on fluxes as a function of the concentration. However, we found that for our application it was necessary to use mixing ratio fluxes, which we will describe in this appendix. We give formulas for first order fluxes, but the extension to third order fluxes is straightforward.

A.1 Splitting with concentrations

We consider the 3D advection equation in conservation form, which reads

$$c_t + (uc)_x + (vc)_y + (wc)_z = 0,$$

with unknown concentration, or vector of concentrations, c. A straightforward way to solve the advection equation numerically is by dimensional splitting. In its most simple form this is

$$c^*_{i,j,k} = c^n_{i,j,k} + \left(F^n_{i-\frac{1}{2},j,k} - F^n_{i+\frac{1}{2},j,k}\right),$$

$$c^{**}_{i,j,k} = c^*_{i,j,k} + \left(G^*_{i,j-\frac{1}{2},k} - G^*_{i,j+\frac{1}{2},k}\right),$$

$$c^{n+1}_{i,j,k} = c^{**}_{i,j,k} + \left(H^{**}_{i,j,k-\frac{1}{2}} - H^{**}_{i,j,k+\frac{1}{2}}\right),$$

with concentration fluxes $F_{i+\frac{1}{2},j,k}$, $G_{i,j+\frac{1}{2},k}$ and $H_{i,j,k+\frac{1}{2}}$ computed by some 1D procedure, using interpolation of concentrations in x, y and z direction, respectively. For example, first-order upwind fluxes are given by

$$F_{i+\frac{1}{2}} = \begin{cases} \nu_{i+\frac{1}{2}} c_{i,j,k} & \text{if} \quad u_{i+\frac{1}{2}} \geq 0, \\ -\nu_{i+\frac{1}{2}} c_{i+1,j,k} & \text{if} \quad u_{i+\frac{1}{2}} < 0 \end{cases}$$

with $\nu_{i+\frac{1}{2}} = |u_{i+\frac{1}{2}}|\Delta t/\Delta x$ the local Courant number at the right cell boundary $(x_{i+\frac{1}{2}}, y_j, z_k)$.

A disadvantage of splitting is the lack of monotonicity, even if the wind field is divergence free and the concentration is constant in space. In the first step one tries to approximate the equation $c_t + (uc)_x = 0$, and to remain consistent monotonicity has to be sacrificed. As observed by *Bott* [1992], first-order splitting may give qualitatively bad results with deformational flow fields. On the other hand, experiments in [*Hundsdorfer and Spee*, 1995] suggested that for advection on a plane much better results are obtained if one uses a genuine second-order splitting method. Here the splitting should be second-order, for example Strang splitting [*Strang*, 1968], but also the 1D processes should be approximated with second-order accuracy. However, tests with advection on a sphere in [*Hundsdorfer and Spee*, 1995] revealed that near the poles additional modifications were required, also with this second-order splitting.

The (2D) modification 'deformation correction' suggested in [*Hundsdorfer and Spee*, 1995], consists of multiplying after each step the concentrations $c^{n+1}_{i,j}$ by a factor $\delta_{i,j}$ such that if we had started with $c^n_{i,j} \equiv 1$ then the $c^{n+1}_{i,j}$ would be the same as the first order, non-splitted, Donorcell algorithm applied to this uniform concentration field. Since this is a modification on the concentrations, not on the fluxes, the resulting scheme is not strictly mass conservative. Some tests in [*Hundsdorfer and Spee*, 1995] on an analytical wind field of *Williamson and Rasch* [1989] gave results which were 'almost' mass conserving. Still this point remained a matter of concern.

A.2 Splitting with mixing ratio fluxes

To overcome the lack of monotonicity a modification on the fluxes was suggested by *Russell and Lerner* [1981]. Our attention on this paper was drawn by the article of *Easter* [1992]. Also *Allen et al.* [1991] proposed a similar approach.

Suppose the wind field is divergence free. Then a constant concentration field at time t_n should still be constant at t_{n+1}. Suppose now that we have given velocities that are divergence free in the discrete form

$$u_{i+\frac{1}{2}} - u_{i-\frac{1}{2}} + v_{j+\frac{1}{2}} - v_{j-\frac{1}{2}} + w_{k+\frac{1}{2}} - w_{k-\frac{1}{2}} = 0.$$

Then, if we have the densities $\rho^n_{i,j,k}$ at time t_n, and use these to compute the fluxes, the values at time t_{n+1} remain constant,

$$\rho^*_{i,j,k} = \rho^n_{i,j,k} + \frac{\tau}{\Delta x}\Big(u_{i+\frac{1}{2}} - u_{i-\frac{1}{2}}\Big),$$

$$\rho^{**}_{i,j,k} = \rho^*_{i,j,k} + \frac{\tau}{\Delta y}\Big(v_{j+\frac{1}{2}} - v_{j-\frac{1}{2}}\Big),$$

$$\rho^{n+1}_{i,j,k} = \rho^{**}_{i,j,k} + \frac{\tau}{\Delta z}\Big(w_{k+\frac{1}{2}} - w_{k-\frac{1}{2}}\Big) \equiv \rho^n_{i,j,k}.$$

This is in spite of the fact that the intermediate results $\rho^*_{i,j,k}$ and $\rho^{**}_{i,j,k}$ may give large variations. Note that the calculation of these intermediate results is similar to what is done in a splitting method.

The splitting modification of *Russell and Lerner* [1981], consist of calculating the fluxes not from the concentrations $c^n_{i,j,k}$ and $c^*_{i,j,k}$, but from the mixing ratios $q_{i,j,k} = c_{i,j,k}/\rho_{i,j,k}$. The resulting scheme is

$$q^n_{i,j,k} = \frac{c^n_{i,j,k}}{\rho^n_{i,j,k}}, \qquad c^*_{i,j,k} = c^n_{i,j,k} + \Big(f^n_{i-\frac{1}{2},j,k} - f^n_{i+\frac{1}{2},j,k}\Big),$$

$$\rho^*_{i,j,k} = \rho^n_{i,j,k} + \frac{\tau}{\Delta x}\Big(u_{i+\frac{1}{2}} - u_{i-\frac{1}{2}}\Big), \qquad q^*_{i,j,k} = \frac{c^*_{i,j,k}}{\rho^*_{i,j,k}}, \qquad c^{**}_{i,j,k} = c^*_{i,j,k} + \Big(g^*_{i,j-\frac{1}{2},k} - g^*_{i,j+\frac{1}{2},k}\Big),$$

$$\rho^{**}_{i,j,k} = \rho^*_{i,j,k} + \frac{\tau}{\Delta y}\Big(v_{j+\frac{1}{2}} - v_{j-\frac{1}{2}}\Big), \qquad q^{**}_{i,j,k} = \frac{c^{**}_{i,j,k}}{\rho^{**}_{i,j,k}}, \qquad c^{n+1}_{i,j,k} = c^{**}_{i,j,k} + \Big(h^{**}_{i,j,k-\frac{1}{2}} - h^{**}_{i,j,k+\frac{1}{2}}\Big),$$

with mixing ratio fluxes $f_{i+\frac{1}{2},j,k}$, $g_{i,j+\frac{1}{2},k}$ and $h_{i,j,k+\frac{1}{2}}$. These are computed by the same way as the concentration fluxes, only the values $q^n_{i,j,k}$, $q^*_{i,j,k}$ and $q^{**}_{i,j,k}$ are now used. For example, first-order upwind fluxes are given by

$$f_{i+\frac{1}{2}} = \begin{cases} \rho_{i+\frac{1}{2}}\,\nu_{i+\frac{1}{2}} q_{i,j,k} & \text{if} \quad u_{i+\frac{1}{2}} \geq 0, \\ -\rho_{i+\frac{1}{2}}\nu_{i+\frac{1}{2}} q_{i+1,j,k} & \text{if} \quad u_{i+\frac{1}{2}} < 0, \end{cases}$$

$$g^*_{j+\frac{1}{2}} = \begin{cases} \rho_{j+\frac{1}{2}}\,\nu_{j+\frac{1}{2}} q^*_{i,j,k} & \text{if} \quad v_{j+\frac{1}{2}} \geq 0, \\ -\rho_{j+\frac{1}{2}}\nu_{j+\frac{1}{2}} q^*_{i,j+1,k} & \text{if} \quad v_{j+\frac{1}{2}} < 0, \end{cases}$$

$$h^{**}_{k+\frac{1}{2}} = \begin{cases} \rho_{k+\frac{1}{2}}\,\nu_{k+\frac{1}{2}} q^{**}_{i,j,k} & \text{if} \quad w_{k+\frac{1}{2}} \geq 0, \\ -\rho_{k+\frac{1}{2}}\nu_{k+\frac{1}{2}} q^{**}_{i,j,k+1} & \text{if} \quad w_{k+\frac{1}{2}} < 0, \end{cases}$$

with $\nu_{j+\frac{1}{2}} = |v_{j+\frac{1}{2}}|\Delta t/\Delta y$ and $\nu_{k+\frac{1}{2}} = |w_{k+\frac{1}{2}}|\Delta t/\Delta z$ the local Courant numbers.

Suppose that the very first step of this algorithm gives $q^n_{i,j,k} = 1$ for all i, j, k. Then the interpolation for the fluxes is trivial, and we get $q^*_{i,j,k} = 1$ since the formulas for $c^{n+1}_{i,j,k}$ and $\rho^{n+1}_{i,j,k}$ will be the same. In a similar way it follows that $q^{n+1}_{i,j,k} = c^{n+1}_{i,j,k}/\rho^{n+1}_{i,j,k} \equiv 1$.

Likewise, if we have a divergence-free wind field together with $c^n_{i,j,k} \equiv 1$, then it follows that $c^{n+1}_{i,j,k} \equiv 1$. This property is not shared by the original splitting. Due to the fact that the intermediate quantities $c^*_{i,j,k}$ may be far from equilibrium, the interpolation in the second step may give large errors in the original splitting. We found almost identical results for analytical wind field as in [*Hundsdorfer and Spee*, 1995].

A.3 Convergence proof

It is not clear a priori whether splitting with the mixing ratio fluxes converges to the correct result. This will be demonstrated here for first-order upwind fluxes with velocities u, v positive, not necessarily divergence free, and with artificial densities $\rho^n_{i,j} \equiv 1$. We give this proof for 2D advection, the extension to 3D is straightforward. Then $q^n_{i,j} = c^n_{i,j}$ and

$$c^*_{i,j} = c^n_{i,j} + \frac{\tau}{\Delta x}\Big(u_{i-\frac{1}{2},j}c^n_{i-1,j} - u_{i+\frac{1}{2},j}c^n_{i,j}\Big),$$

$$q^*_{i,j} = c^*_{i,j}/\rho^*_{i,j} \qquad \text{with} \qquad \rho^*_{i,j} = 1 + \frac{\tau}{\Delta x}\left(u_{i-\frac{1}{2}} - u_{i+\frac{1}{2}}\right),$$

$$c^{n+1}_{i,j} = c^*_{i,j} + \frac{\tau}{\Delta y}\Big(v_{j-\frac{1}{2}}q^*_{i,j-1} - v_{j+\frac{1}{2}}q^*_{i,j}\Big).$$

This last formula can also be written as

$$c^{n+1}_{i,j} = c^*_{i,j} + \frac{\tau}{\Delta y}\Big(v^*_{j-\frac{1}{2}}c^*_{i,j-1} - v^*_{j+\frac{1}{2}}c^*_{i,j}\Big),$$

with $v^*_{j+\frac{1}{2}} = v_{j+\frac{1}{2}}/\rho^*_{i,j}$. Note that

$$\rho^*_{i,j} = 1 + \frac{\tau}{\Delta x}\Big(u_{i-\frac{1}{2},j} - u_{i+\frac{1}{2},j}\Big) \approx 1 + \tau u_x(x_i, y_j).$$

So, the above procedure is equivalent with first-order upwind splitting in terms of the concentrations, but with a modified velocity

$$u^* = u, \qquad v^* = \frac{v}{1 + \tau(u_x + \mathcal{O}(\Delta x))} = (1 + \mathcal{O}(\tau))\ v.$$

First-order upwind splitting with these velocities will approximate the exact solution of $c^*_t = (u^*c^*)_x + (v^*c^*)_y$ with a global error $\mathcal{O}(h)$, where $h = \max(\Delta x, \Delta y)$. Further the difference of $c(x, y, t)$ and $c^*(x, y, t)$ is of $\mathcal{O}(\tau)$. Thus the above scheme approximates $c(x, y, t)$ with an error $\mathcal{O}(\tau) + \mathcal{O}(h)$. Note that it has not been assumed that the wind field is divergence free.